

# CONSTRAINTS ON THE SPACETIME GEOMETRY AROUND 10 STELLAR-MASS BLACK HOLE CANDIDATES FROM THE DISK'S THERMAL SPECTRUM

LINGYAO KONG, ZILONG LI, AND COSIMO BAMBI<sup>a</sup>

Center for Field Theory and Particle Physics & Department of Physics, Fudan University, 200433 Shanghai, China

*Draft version December 3, 2024*

## ABSTRACT

In a previous paper, one of us has described a code to compute the thermal spectrum of geometrically thin and optically thick accretion disks around generic stationary and axisymmetric black holes, which are not necessarily of the Kerr type. As the structure of the accretion disk and the propagation of electromagnetic radiation from the disk to the distant observer depend on the background metric, the analysis of the thermal spectrum of thin disks can be used to constrain the geometry of the spacetime around these objects. In this paper, we consider the 10 stellar-mass black hole candidates for which the spin parameter has been already estimated from the analysis of the disk's thermal spectrum and under the assumption of the Kerr background, and we translate the measurements reported in the literature into an allowed region on the spin–deformation parameters plane. The analysis of the disk's thermal spectrum can be used to estimate only one parameter of the geometry close to the compact object, and therefore it is not possible to get independent constraints of both the spin and the deformation parameters, but only of a certain combination of them. The constraints obtained here will be used in combination with other measurements in future work, with the final goal to break the degeneracy between the spin and possible deviations from the Kerr solution and thus test the Kerr nature of astrophysical black hole candidates.

*Subject headings:* accretion, accretion disks — black hole physics — gravitation — X-rays: binaries

## 1. INTRODUCTION

General relativity makes very clear predictions about the properties of the spacetime geometry around a black hole (BH). According to the no-hair theorem (Carter 1971; Robinson 1975; Chruściel et al. 2012), 4-dimensional uncharged BHs are only described by the Kerr solution, which is completely specified by two parameters, associated respectively with the mass  $M$  and the spin angular momentum  $J$  of the compact object.  $M$  and  $J$  cannot be completely arbitrary, but they must satisfy the condition  $|a_*| \leq 1$ , where  $a_* = J/M^2$  is the spin parameter. For  $|a_*| > 1$ , there is no event horizon and there is a number of theoretical arguments suggesting that such super-spinning Kerr objects can unlikely be relevant in astrophysics (Dotti et al. 2008; Pani et al. 2010; Barausse et al. 2010; Giacomazzo et al. 2011).

From the observational side, there are at least two classes of astrophysical BH candidates: stellar-mass objects in X-ray binary systems ( $M \approx 5 - 20 M_\odot$ ) (Remillard & McClintock 2006), and super-massive BH candidates at the center of every normal galaxy ( $M \sim 10^5 - 10^9 M_\odot$ ) (Kormendy & Richstone 1995). All these objects are thought to be the Kerr BHs of general relativity simply because they cannot be explained otherwise without introducing new physics. Stellar-mass BH candidates are too heavy to be neutron or quark stars for any reasonable matter equation of state (Rhoades & Ruffini 1974; Kalogera & Baym 1996). At least some super-massive BH candidates in galactic nuclei are definitively too massive, compact, and old to be clusters of non-luminous bodies, as the cluster lifetime due to evaporation and physical collisions would be shorter than the age of these systems (Maoz 1998). For both stellar-mass and super-massive BH candidates, there is no evidence of electromagnetic radiation emitted by their surface, which may be interpreted as an indication for the presence of an event/apparent horizon (Narayan & Heyl 2002; McClintock et al. 2004; Narayan & McClintock 2008; Broderick et al. 2009).

Despite this body of indirect evidence, there is no indication that the spacetime geometry around BH candidates is described by the Kerr metric. The Kerr BH hypothesis entirely relies on the validity of standard physics. The no-hair theorem might be avoided by a number of ways, such as by considering exotic forms of matter, non-stationary solutions, or non-trivial extensions of general relativity. It is therefore of extreme importance to experimentally test the Kerr nature of astrophysical BH candidates and, thanks to the progresses in the last decade in the understanding of the accretion processes and in the observational facilities, such a possibility is not out of reach any more [for a review, see e.g. Bambi (2011, 2013b)]. This goal can be achieved by extending the techniques that have been developed to estimate the spin parameter of BH candidates under the assumption that they are of the Kerr type. The compact object is now specified by a mass  $M$ , a spin parameter  $a_*$ , and at least one deformation parameter, which measures possible deviations from the Kerr geometry. One then computes the observational features in this more general background. The comparison of the theoretical predictions with the observational data is now used to estimate both the spin and the deformation parameters. If one finds a vanishing deformation parameter, the Kerr BH hypothesis is verified. If the observational data point out a non-vanishing deformation parameter, the Kerr nature of astrophysical BH candidates is questioned. However, even assuming to have the correct theoretical model and all the systematic effects under control,

<sup>a</sup> Corresponding author: bambi@fudan.edu.cn

there is a problem preventing to arrive at a final conclusion. It turns out that there is a strong correlation between the estimate of the spin and of the deformation parameter, so that the final result is usually an allowed region on the spin–deformation parameters plane. The reason is that the measurement of a specific feature of the electromagnetic spectrum can only infer one parameter of the background metric close to the compact object. The strategy is therefore to combine different measurements of the same object and break this degeneracy, identifying a limited area on the spin–deformation parameters plane. With a single measurement, we can only rule out some BH alternatives with very specific features, like some exotic compact objects without event horizon (Bambi & Malafarina 2013; Joshi et al. 2014) and some wormholes (Bambi 2013c), or constrain the deformation parameter in classes of non-Kerr BHs that can mimic fast-rotating Kerr BHs only for a restricted ranges of the spin and of the deformation parameters (Bambi 2014).

At present, the most robust technique to probe the spacetime geometry around stellar-mass BH candidates is probably the continuum-fitting method; that is, the analysis of the thermal spectrum of geometrically thin and optically thick accretion disks (Zhang et al. 1997). In the case of Kerr BHs, the thermal spectrum of thin accretion disks depends on 5 free parameters; that is, the BH mass  $M$ , the BH spin parameter  $a_*$ , the mass accretion rate  $\dot{M}$ , the BH distance  $d$ , and the inclination angle  $i$  of the disk with respect to the line of sight of the distant observer. As put forward in Zhang et al. (1997), if we have independent measurements of  $M$ ,  $d$ , and  $i$ , the analysis of the disk’s thermal spectrum can provide an estimate of  $a_*$  and  $\dot{M}$ . This approach has been extensively discussed in the literature, its assumptions and limitations well investigated and tested at both theoretical and observational level, and up to now the spin parameter has been measured for about 10 stellar-mass BH candidates with this technique (Li et al. 2005; McClintock et al. 2011, 2013). The continuum-fitting method cannot be used in the case of supermassive objects because the disk’s temperature goes like  $M^{-0.25}$ , and for  $M \sim 10^5 - 10^9 M_\odot$  the peak falls in the optical/UV range, where dust absorption prevents good observations. The analysis of the disk’s thermal spectrum can be naturally extended to non-Kerr spacetimes to test the Kerr nature of astrophysical BH candidates (Bambi & Barausse 2011; Bambi 2012e).

In the present paper, we will use the code described in Bambi (2012e) to constrain the spin and the deformation parameters of the 10 stellar-mass BH candidates in X-ray binary systems for which the continuum-fitting method has already been used by other authors to get an estimate of the spin parameter under the assumption that these objects are Kerr BHs. Our code is based on a ray-tracing approach and includes all the special and general relativistic effects. The natural way to obtain these constraints would be to start from the raw data and repeat the complete data analysis for each object, with the sole difference that the thermal spectrum is now computed in a more general metric that includes the Kerr solution as special case. While this would be surely the correct way to proceed, here we will perform a simplified analysis in which, significantly reducing the time of the analysis as well as the complications related to a large number of systematic effects, we will not lose any important information. The idea is to compare the Kerr spectra with the spin parameters reported in the literature with the spectra computed in our generic spacetime with a possible non-vanishing deformation parameter. The approach makes sense because the thermal spectrum of a thin disk around a non-Kerr BH with a certain spin and deformation parameters is extremely similar to the one around a Kerr BH with different spin and that remains true even for quite large deviations from the Kerr solution. In other words, it is impossible even in principle to distinguish a Kerr BH and a non-Kerr BH from the sole analysis of the disk’s thermal spectrum (Bambi 2012e, 2014) and therefore we can assume as reference spectrum the one of a Kerr BH with the spins reported in the literature. This approach significantly simplify our job because we can just focus our attention on the role of the spacetime metric, assuming that all the astrophysical effects and the instrumental issues have been already properly taken into account in the previous studies. Our work is the first step of a project that aims at testing the Kerr nature of BH candidates: the measurements reported in the present paper will be combined with other observations to try to break the degeneracy between the spin and the deformation parameters, thus finding a limited allowed region on the spin–deformation parameters plane. We note that the use of the measurements from the continuum-fitting method and their combinations with other observations have already been studied in previous papers (Bambi 2012b,c,d). However, those constraints on the spin–deformation parameters plane were obtained with some simplifications (that, as we will show here, provide a quite correct measurement for small inclination angles and not near-extremal BHs, while there are some deviations from the right result in the case the disk is almost edge-on or the Kerr spin measurement is close to 1). Here we will remove such a set of simplifications and we will obtain the most reliable constraints possible with current knowledge.

The content of the paper is as follows. In Section 2, we review the calculations of the thermal spectrum of geometrically thin and optically thick accretion disks around generic stationary and axisymmetric BHs. In Section 3, we present our approach and we find the allowed region on the spin-deformation parameters plane for each of the 10 stellar-mass BH candidates for which a robust spin measurement from the disk’s thermal spectrum has been reported in the literature. In Section 4, we discuss our results. Summary and conclusions are reported in Section 5. Throughout the paper, we use units in which  $G_N = c = 1$ , unless stated otherwise.

## 2. THERMAL SPECTRUM OF THIN DISKS

The standard framework to describe geometrically thin and optically thick accretion disks is the Novikov-Thorne model (Novikov & Thorne 1973; Page & Thorne 1974), which is the relativistic generalization of the Shakura-Sunyaev

one (Shakura & Sunyaev 1973). Accretion is possible because viscous magnetic/turbulent stresses and radiation transport energy and angular momentum outward. In a generic stationary, axisymmetric, and asymptotically flat spacetime, the model assumes that the disk is on the equatorial plane, that the disk's gas moves on nearly geodesic circular orbits, and that the radial heat transport is negligible compared to the energy radiated from the disk's surface. From the conservation laws for the rest-mass, angular momentum and energy, one can deduce three basic equations for the time-averaged radial structure of the disk (Page & Thorne 1974). These equations determine the radius-independent time-averaged mass accretion rate  $\dot{M}$ , the time-averaged energy flux  $\mathcal{F}(r)$  from the surface of the disk (as measured by an observer comoving with the disk's gas) and the time-average torque  $W_\phi^r(r)$ :

$$\dot{M} = -2\pi\sqrt{-G}\Sigma u^r = \text{const.}, \quad (1)$$

$$\mathcal{F}(r) = \frac{\dot{M}}{4\pi M^2} F(r), \quad (2)$$

$$W_\phi^r(r) = \frac{\dot{M}}{2\pi M^2} \frac{\Omega L_z - E}{\partial_r \Omega} F(r), \quad (3)$$

where  $\Sigma$  is the surface density,  $u^r$  is the radial 4-velocity,  $G = -\alpha^2 g_{rr} g_{\phi\phi}$  is the determinant of the near equatorial plane metric in cylindrical coordinates, and  $\alpha^2 = g_{t\phi}^2/g_{\phi\phi} - g_{tt}$  is the lapse function.  $E$ ,  $L_z$ , and  $\Omega$  are, respectively, the conserved specific energy, the conserved  $z$ -component of the specific angular momentum, and the angular velocity  $d\phi/dt$  for equatorial circular geodesics.  $F(r)$  is given by

$$F(r) = -\frac{\partial_r \Omega}{(E - \Omega L_z)^2} \frac{M^2}{\sqrt{-G}} \int_{r_{\text{in}}}^r (E - \Omega L_z) (\partial_\rho L_z) d\rho, \quad (4)$$

where  $r_{\text{in}}$  is the inner radius of the accretion disk and in the Novikov-Thorne model it is supposed to be the radius of the innermost stable circular orbit (ISCO). The calculation of  $E$ ,  $L_z$ , and  $\Omega$  in a generic stationary and axisymmetric spacetime can be found, for instance, in Appendix B of Bambi & Barausse (2011).

Since the disk is in thermal equilibrium, the emission is blackbody-like and we can define an effective temperature  $T_{\text{eff}}(r)$  from the relation  $\mathcal{F}(r) = \sigma T_{\text{eff}}^4$ , where  $\sigma$  is the Stefan-Boltzmann constant. Actually, the disk's temperature near the inner edge of the disk can be high, up to  $\sim 10^7$  K for stellar-mass BH candidates, and non-thermal effects are non-negligible. That is usually taken into account by introducing the color factor (or hardening factor)  $f_{\text{col}}$ . The color temperature is  $T_{\text{col}}(r) = f_{\text{col}} T_{\text{eff}}$  and the local specific intensity of the radiation emitted by the disk is

$$I_e(\nu_e) = \frac{2h\nu_e^3}{c^2} \frac{1}{f_{\text{col}}^4} \frac{\Upsilon}{\exp\left(\frac{h\nu_e}{k_B T_{\text{col}}}\right) - 1}, \quad (5)$$

where  $\nu_e$  is the photon frequency,  $h$  is the Planck's constant,  $c$  is the speed of light,  $k_B$  is the Boltzmann constant, and  $\Upsilon$  is a function of the angle between the wavevector of the photon emitted by the disk and the normal of the disk surface, say  $\xi$ . The two most common choices are  $\Upsilon = 1$  (isotropic emission) and  $\Upsilon = \frac{1}{2} + \frac{3}{4} \cos \xi$  (limb-darkened emission).

The calculation of the thermal spectrum of Novikov-Thorne disks has been extensively discussed in the literature, see e.g. Li et al. (2005) and references therein. We consider the observer's image plane with Cartesian coordinates  $(X, Y)$ . Photons emitted from the disk that reach the distant observer hit the observer's image plane with 3-momentum perpendicular to the latter. If we numerically integrate the photon trajectory backwards in time to the point of the photon emission on the accretion disk, we find the radial coordinate  $r_e$  at which the photon was emitted and the angle  $\xi$  between the wavevector of the photon and the normal of the disk surface (necessary to compute  $\Upsilon$ ). If the image plane of the distant observer is divided into a number of small elements, the ray-tracing procedure provides the observed flux density from each element. Summing up all the elements, we get the total observed flux density of the disk. The photon flux number density is given by

$$N_{E_{\text{obs}}} = \frac{1}{E_{\text{obs}}} \int I_{\text{obs}}(\nu) d\Omega_{\text{obs}} = \frac{1}{E_{\text{obs}}} \int g^3 I_e(\nu_e) d\Omega_{\text{obs}} = A_1 \left(\frac{E_{\text{obs}}}{\text{keV}}\right)^2 \int \frac{1}{M^2} \frac{\Upsilon dX dY}{\exp\left[\frac{A_2}{g^{F^{1/4}}}\left(\frac{E_{\text{obs}}}{\text{keV}}\right)\right] - 1}, \quad (6)$$

where  $I_{\text{obs}}$ ,  $E_{\text{obs}}$ , and  $\nu$  are, respectively, the specific intensity of the radiation, the photon energy, and the photon frequency measured by the distant observer.  $I_e(\nu_e)/\nu_e^3 = I_{\text{obs}}(\nu)/\nu^3$  follows from the Liouville theorem.  $d\Omega_{\text{obs}} = dX dY/d^2$  is the element of the solid angle subtended by the image of the disk on the observer's sky,  $d$  is the distance of the source, and  $A_1$  and  $A_2$  are given by

$$A_1 = \frac{2(\text{keV})^2}{f_{\text{col}}^4} \left(\frac{G_N M}{c^3 h d}\right)^2 = \frac{0.07205}{f_{\text{col}}^4} \left(\frac{M}{M_\odot}\right)^2 \left(\frac{\text{kpc}}{d}\right)^2 \gamma \text{keV}^{-1} \text{cm}^{-2} \text{s}^{-1},$$

$$A_2 = \left(\frac{\text{keV}}{k_B f_{\text{col}}}\right) \left(\frac{G_N M}{c^3}\right)^{1/2} \left(\frac{4\pi\sigma}{\dot{M}}\right)^{1/4} = \frac{0.1331}{f_{\text{col}}} \left(\frac{10^{18} \text{g s}^{-1}}{\dot{M}}\right)^{1/4} \left(\frac{M}{M_\odot}\right)^{1/2}. \quad (7)$$

$g$  is the redshift factor

$$g = \frac{\nu}{\nu_e} = \frac{k_\mu u_o^\mu}{k_\mu u_e^\mu}, \quad (8)$$

where  $u_o^\mu = (-1, 0, 0, 0)$  is the 4-velocity of the observer and  $u_e^\mu = (u_e^t, 0, 0, \Omega u_e^t)$  is the 4-velocity of the emitter. Using the normalization condition  $g_{\mu\nu} u_e^\mu u_e^\nu = -1$ ,  $u_e^t$  can be written as

$$u_e^t = \frac{1}{\sqrt{-g_{tt} - 2g_{t\phi}\Omega - g_{\phi\phi}\Omega^2}}. \quad (9)$$

Because the  $t$ - and  $\phi$ -component of a photon's canonical 4-momentum are conserved quantities in any stationary and axisymmetric spacetime, the constant  $k_\phi/k_t = \lambda$  can be calculated from the photon initial conditions on the observer's image plane and

$$g = \frac{\sqrt{-g_{tt} - 2g_{t\phi}\Omega - g_{\phi\phi}\Omega^2}}{1 + \lambda\Omega}. \quad (10)$$

With  $g$ , we take into account the special and general relativistic effects of Doppler boost and gravitational redshift. The effect of light bending is included in the ray-tracing calculation.

### 3. CONSTRAINTS ON POSSIBLE DEVIATIONS FROM THE KERR GEOMETRY

The formalism reviewed in the previous section is very general, in the sense that it can be applied for any stationary, axisymmetric, and asymptotically flat spacetime. In the special case of the Kerr background, the ray-tracing part of the calculation of the photon trajectories from the disk to the observer's image plane can be significantly simplified, because the spacetime is of Petrov type D and in Boyer-Lindquist coordinates the photon equations of motion are separable and of first order. This is not true in the general case, and our code solves the second order photon geodesic equations. As background geometry, here we adopt the Johannsen-Psaltis metric, which was explicitly proposed in Johannsen & Psaltis (2011b) to test the geometry around BH candidates. In Boyer-Lindquist coordinates, the line element is (Johannsen & Psaltis 2011b)

$$ds^2 = - \left(1 - \frac{2Mr}{\Sigma}\right) (1+h) dt^2 - \frac{4aMr \sin^2 \theta}{\Sigma} (1+h) dt d\phi + \frac{\Sigma(1+h)}{\Delta + a^2 h \sin^2 \theta} dr^2 + \Sigma d\theta^2 + \left[ \sin^2 \theta \left( r^2 + a^2 + \frac{2a^2 Mr \sin^2 \theta}{\Sigma} \right) + \frac{a^2 (\Sigma + 2Mr) \sin^4 \theta}{\Sigma} h \right] d\phi^2, \quad (11)$$

where

$$\begin{aligned} \Sigma &= r^2 + a^2 \cos^2 \theta, \\ \Delta &= r^2 - 2Mr + a^2, \\ h &= \sum_{k=0}^{\infty} \left( \epsilon_{2k} + \frac{Mr}{\Sigma} \epsilon_{2k+1} \right) \left( \frac{M^2}{\Sigma} \right)^k. \end{aligned} \quad (12)$$

This metric has an infinite number of deformation parameters  $\epsilon_i$  and the Kerr solution is recovered when all the deformation parameters vanish. However, in order to reproduce the correct Newtonian limit, we have to impose  $\epsilon_0 = \epsilon_1 = 0$ , while  $\epsilon_2$  is strongly constrained by Solar System experiments (assuming the validity of the Birkhoff theorem). In the rest of this paper, we restrict our attention to the deformation parameter  $\epsilon_3$  and set to zero all the others. Such a simplification does not imply a significant loss of information, because eventually all the deformation parameters introduce the same effects (Bambi 2012a). For  $\epsilon_i > 0$ , the BH is more oblate than its Kerr counterpart with the same spin and the gravitational force on the equatorial plane is weaker. For  $\epsilon_i < 0$ , the BH is more prolate than the Kerr one and the gravitational force on the equatorial plane is stronger. The key-point in the continuum-fitting method is the position of the ISCO radius, which sets the inner edge of the accretion disk. The combination of several deformation parameters makes the analysis more complicated, but it does not introduce important new physics. In the end, at first approximation, when we want to test the Kerr geometry around a BH candidate we want to figure out if the gravitational force around the compact object is stronger or weaker than the one expected in a Kerr background with the same spin parameter. At the present stage, this is the best we can do, while more specific deviations from the Kerr solution only introduce smaller corrections. Let us also note that the metric in Eq. (11) is not the most general non-Kerr background, and there are efforts to generalize it (Cardoso et al. 2014). Despite that, for our purpose it makes sense to consider the simplest case – which is already difficult to constrain – and the same theoretical framework will be used in future work.

With the metric in Eq. (11), we can compute the expected thermal spectrum of thin accretion disks and compare the results with observational data (in the present paper, with the theoretical spectra in Kerr background with the

BH Binary	$M/M_{\odot}$	$i$	$a_*$	Reference
GRO J1655-40	$6.30 \pm 0.27$	$70.2^{\circ} \pm 1.2^{\circ}$	$0.70 \pm 0.10$	Shafee et al. (2006)
4U 1543-47	$9.4 \pm 1.0$	$20.7^{\circ} \pm 1.5^{\circ}$	$0.80 \pm 0.10$	Shafee et al. (2006)
GRS 1915+105	$14.0 \pm 4.4$	$66^{\circ} \pm 2^{\circ}$	$> 0.98$	McClintock et al. (2006)
M33 X-7	$15.65 \pm 1.45$	$74.6^{\circ} \pm 1.0^{\circ}$	$0.84 \pm 0.05$	Liu et al. (2008, 2010)
LMC X-1	$10.91 \pm 1.54$	$36.38^{\circ} \pm 2.02^{\circ}$	$0.92^{+0.05}_{-0.07}$	Gou et al. (2009)
A0620-00	$6.61 \pm 0.25$	$51.0^{\circ} \pm 0.9^{\circ}$	$0.12 \pm 0.19$	Gou et al. (2010)
XTE J1550-564	$9.10 \pm 0.61$	$74.7^{\circ} \pm 3.8^{\circ}$	$0.34^{+0.20}_{-0.28}$	Steiner et al. (2011)
Cygnus X-1	$14.8 \pm 1.0$	$27.1^{\circ} \pm 0.8^{\circ}$	$> 0.98$	Gou et al. (2011, 2013)
H1743-322	$\sim 10$	$75^{\circ} \pm 3^{\circ}$	$0.2 \pm 0.3$	Steiner et al. (2012)
LMC X-3	$6.95 \pm 0.33$	$69.6^{\circ} \pm 0.6^{\circ}$	$0.21 \pm 0.12$	Steiner et al. (2014)
GX 339-4	$5.8 - 15$	$20^{\circ} - 70^{\circ}$	$< 0.9$	Kolehmainen & Done (2010)
GS 1124-683	$7.24 \pm 0.70$	$54^{\circ} \pm 1.5^{\circ}$	$< -0.2$	Morningstar et al. (2014)
M31 microquasar	$\sim 10$	$\sim 32^{\circ}, \sim 39^{\circ}$	$< -0.2$	Middleton et al. (2014)

TABLE 1

CONTINUUM-FITTING MEASUREMENTS OF THE SPIN PARAMETER OF STELLAR-MASS BH CANDIDATES REPORTED IN THE LITERATURE UNDER THE ASSUMPTION OF THE KERR BACKGROUND. SEE THE REFERENCES IN THE LAST COLUMN FOR MORE DETAILS.

same spin parameters as the ones obtained by other authors by fitting X-ray data). The goal is to find an allowed region on the spin–deformation parameters plane. Let us note that, strictly speaking, this approach can only test the Kerr geometry around a BH candidate and does not test the validity of Einstein equations. Indeed, while the Kerr metric is the only vacuum BH solution in 4-dimensional general relativity, it is a solution even in other theories of gravity (Psaltis et al. 2008). Our approach cannot distinguish a Kerr BH of general relativity from a Kerr BH in another theory of gravity because we study the properties of the radiation emitted by a thin disk, which only depend on the background metric, not on the field equations. If we wanted to test the Einstein equations, we should study phenomena like the emission of gravitational waves in the Kerr background (Barausse & Sotiriou 2008).

Tab. 1 shows the spin measurements from the continuum-fitting method reported in the literature and obtained assuming the Kerr nature of the BH candidates. The first column reports the name of the binary system, the second column shows the mass measurement of the BH candidates, the third column is for the estimate of the inclination angle of the disk, the fourth column reports the spin measurement, and the fifth column is for the reference of the spin measurement. The BH mass  $M$  and the inclination angle of the disk  $i$  are usually inferred with dynamical models and optical observations, as they are input parameters in the continuum-fitting approach. In some cases, the angle  $i$  is estimated from the orientation of the BH jet, assuming that it is parallel to the BH spin and perpendicular to the accretion disk. See the original papers for more details and McClintock et al. (2011, 2013) for a general discussion. In what follows, we only consider the first 10 BH candidates in this table, while we neglect the last 3. The constraint on the spin parameter of the BH candidate in GX 339-4 is so weak that this object is completely useless for our purpose. The two recent studies of GS 1124-683 and of the microquasar in M31 seem to indicate that the accretion disk of these objects is counterrotating, but in this case the applicability of the continuum-fitting method is more questionable. So we prefer to focus our attention only on those measurements that are supposed to be the most robust and reliable, at least according to our present understanding.

Figs. 1-3 show the constraints on the spin–deformation parameters plane for these 10 stellar mass BH candidates. They have been obtained in the following way. We have assumed as “reference spectrum” the one of a Kerr BH with spin parameter given by the central value in Tab. 1. We have then computed the  $\chi^2$  by comparing the reference spectrum with the one of a Johannsen-Psaltis BH with spin parameter  $a_*$  and deformation parameter  $\epsilon_3$ . This is the same approach described and used in Bambi & Barausse (2011). The other input parameters are the same, because they have to be determined by independent measurements. In particular, the disk’s inclination angle  $i$  is the central value shown in the third column of Tab. 1 for any object. In the continuum-fitting method, the mass accretion rate is an output parameter to be inferred during the fitting procedure. Since we eventually measure the accretion luminosity  $L_{\text{acc}} = \eta \dot{M}$ , where  $\eta = 1 - E_{\text{ISCO}}$  is the radiative efficiency in the Novikov-Thorne model and  $E_{\text{ISCO}}$  is the specific energy at the ISCO radius, the mass accretion rate used to compute the spectrum of the BH with spin  $a_*$  and deformation parameter  $\epsilon_3$  is (Bambi & Barausse 2011)

$$\dot{M}(a_*, \epsilon_3) = \frac{\eta_0}{\eta(a_*, \epsilon_3)} \dot{M}_0, \quad (13)$$

where  $\eta_0$  is the radiative efficiency of the reference Kerr BH and  $\dot{M}_0$  is its mass accretion rate. Actually, the exact values of  $\eta_0$  and  $\dot{M}_0$  is completely irrelevant for our calculations because in the end they are a constant, so the important point is that  $\dot{M}(a_*, \epsilon_3)$  scales as the inverse of  $\eta(a_*, \epsilon_3)$ .

In Figs. 1-3, the red-solid lines are the local minima of our  $\chi^2$  for a fixed  $\epsilon_3$ , say  $\chi^2_{\text{min}}(\epsilon_3)$ . For  $\epsilon_3 = 0$ , the minimum of  $\chi^2$  is exactly zero, by definition, but it is usually very close to zero even for a non-vanishing  $\epsilon_3$ . Let us call  $\sigma_-$  and  $\sigma_+$  the value of  $\chi^2$  for  $\epsilon_3 = 0$  corresponding, respectively, to the 1-sigma lower and upper measurements of the BH spin parameter in Tab. 1. For instance, in the case of GRO J1655-40,  $\sigma_- = \chi^2(a_* = 0.6, \epsilon_3 = 0)$  and  $\sigma_+ = \chi^2(a_* = 0.8, \epsilon_3 = 0)$ . The blue-dashed lines in Figs. 1-3 separate BHs with  $\chi^2$  lower than  $\sigma_-$  and  $\sigma_+$  from the one with higher  $\chi^2$ . In particular, the regions on the left side of the red-solid lines and between the red-solid lines

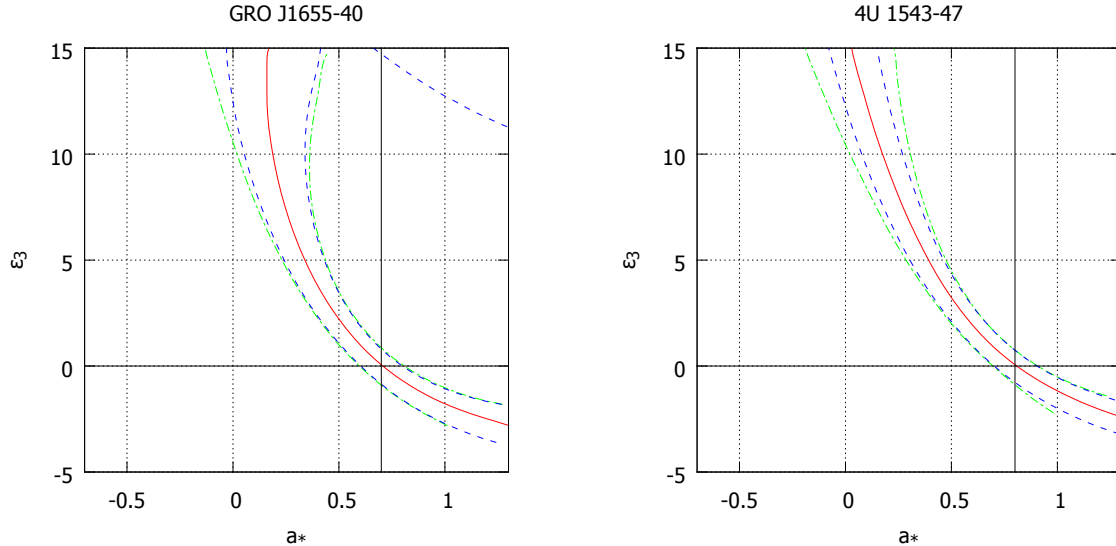


FIG. 1.— Disk’s thermal spectrum constraints on possible deviations from the Kerr geometry in the spacetime around the BH candidates in GRO J1655-40 (left panel) and 4U 1543-47 (right panel). Here and in the other plots of this paper, the red-solid curve is  $\chi^2_{\min}(\epsilon_3)$ , the blue-dashed curves are  $\sigma_-$  and  $\sigma_+$ , respectively on the left and right side of the red-solid line, while the green-dashed-dotted curves are  $\chi^2_{\min}(\epsilon_3) + \sigma_-$  and  $\chi^2_{\min}(\epsilon_3) + \sigma_+$ , respectively on the left and right side of the red-solid line. See the text for more details.

BH Binary	$a_*$					
	$\epsilon_3 = -2$	$\epsilon_3 = 2$	$\epsilon_3 = 4$	$\epsilon_3 = 6$	$\epsilon_3 = 8$	$\epsilon_3 = 10$
GRO J1655-40	$1.04_{-0.18}$	$0.51 \pm 0.09$	$0.38 \pm 0.10$	$0.29 \pm 0.11$	$0.23 \pm 0.14$	$0.19 \pm 0.17$
4U 1543-47	$1.18_{-0.23}$	$0.59 \pm 0.08$	$0.45 \pm 0.09$	$0.34 \pm 0.11$	$0.25 \pm 0.12$	$0.17 \pm 0.15$
GRS 1915+105	—	$> 0.71$	$0.62 < a_* < 1.04$	—	—	—
M33 X-7	—	$0.62 \pm 0.05$	$0.51 \pm 0.05$	$0.45^{+0.05}_{-0.08}$	$0.43^{+0.05}_{-0.11}$	$0.43^{+0.07}_{-0.13}$
LMC X-1	—	$0.68^{+0.02}_{-0.07}$	$0.56^{+0.04}_{-0.08}$	$0.48^{+0.06}_{-0.10}$	$0.43^{+0.08}_{-0.14}$	$0.39^{+0.10}_{-0.18}$
A0620-00	$0.27 \pm 0.22$	$-0.01 \pm 0.18$	$-0.13 \pm 0.18$	$-0.24 \pm 0.19$	$-0.33 \pm 0.18$	$-0.43 \pm 0.18$
XTE J1550-564	$0.52^{+0.25}_{-0.33}$	$0.19^{+0.18}_{-0.27}$	$0.07^{+0.18}_{-0.27}$	$-0.03^{+0.18}_{-0.28}$	$-0.13^{+0.20}_{-0.28}$	$-0.21^{+0.22}_{-0.30}$
Cygnus X-1	—	$> 0.70$	—	—	—	—
H1743-322	$0.36 \pm 0.35$	$0.06 \pm 0.29$	$-0.05 \pm 0.29$	$-0.16 \pm 0.28$	$-0.26 \pm 0.30$	$-0.34 \pm 0.31$
LMC X-3	$0.37 \pm 0.14$	$0.07 \pm 0.12$	$-0.04 \pm 0.12$	$-0.15 \pm 0.12$	$-0.25 \pm 0.12$	$-0.33 \pm 0.12$

TABLE 2

CONTINUUM-FITTING MEASUREMENTS OF THE SPIN PARAMETER OF THE 10 STELLAR-MASS BH CANDIDATES CONSIDERED IN THIS PAPER IN THE CASE THESE OBJECTS ARE JOHANNSEN-PSALTIS BHs WITH SPIN PARAMETER  $\epsilon_3 = -2$  (SECOND COLUMN), 2 (THIRD COLUMN), 4, (FOURTH COLUMN), 6 (FIFTH COLUMN), 8 (SIXTH COLUMN), AND 10 (SEVENTH COLUMN). SEE THE TEXT FOR MORE DETAILS.

and the blue-dashed lines include BHs with  $0 < \chi^2 < \sigma_-$ . The regions on the right hand side of the red-solid lines and between the red-solid lines and the blue-dashed lines are for BHs with  $0 < \chi^2 < \sigma_+$ . It is clear that the objects with  $a_*$  and  $\epsilon_3$  between the two blue-dashed lines are indistinguishable from a Kerr BH with the reference spin within the current uncertainties. Lastly, Figs. 1-3 also show green-dashed-dotted lines for  $\chi^2_{\min}(\epsilon_3) + \sigma_-$  and  $\chi^2_{\min}(\epsilon_3) + \sigma_+$ , respectively on the left and right sides of the red-solid lines.

In most plots, the blue-dashed lines and the green-dashed-dotted lines almost coincide, because  $\chi^2_{\min}(\epsilon_3)$  is very close to zero and the difference between the spectra in Kerr and Johannsen-Psaltis BHs is definitively small. In the cases of the BH candidates in M33 X-7 and LMC X-1, this is not true, especially for high values of the deformation parameter  $\epsilon_3$ . For M33 X-7, we find two local minima of  $\chi^2$  for  $7 < \epsilon_3 < 13$  in the range of our spin-deformation parameters plane. It turns out that, roughly speaking, the disk thermal spectrum of the BHs inside the internal blue-dashed line looks more like the one of Kerr BHs with spin parameter larger than the upper bound inferred assuming the Kerr background,  $a_* = 0.89$ . The spectrum of the BHs outside the external blue-dashed line is more similar to the one of Kerr BHs with spin parameter lower than the lower bound inferred assuming the Kerr metric,  $a_* = 0.79$ . If we assume the Kerr background and we analyze the X-ray data of the thermal spectrum of a thin disk in a Johannsen-Psaltis background located outside the exterior blue-dashed, we would obtain a lower spin parameter than the one measured. The blue-dashed lines are not exactly the lines of BHs with spectrum that looks like the one of a Kerr BH with spin  $a_* = 0.79$  and  $0.89$ , because they have been defined in a different way, but at first approximation they can be thought so. This means that the red-solid line makes sense only up to the point of connection between the two local minima, at  $\epsilon_3 = 13$ , and that the 1-sigma bound  $a_* > 0.79$  obtained in the Kerr background imply something like  $\epsilon_3 < 14$ .

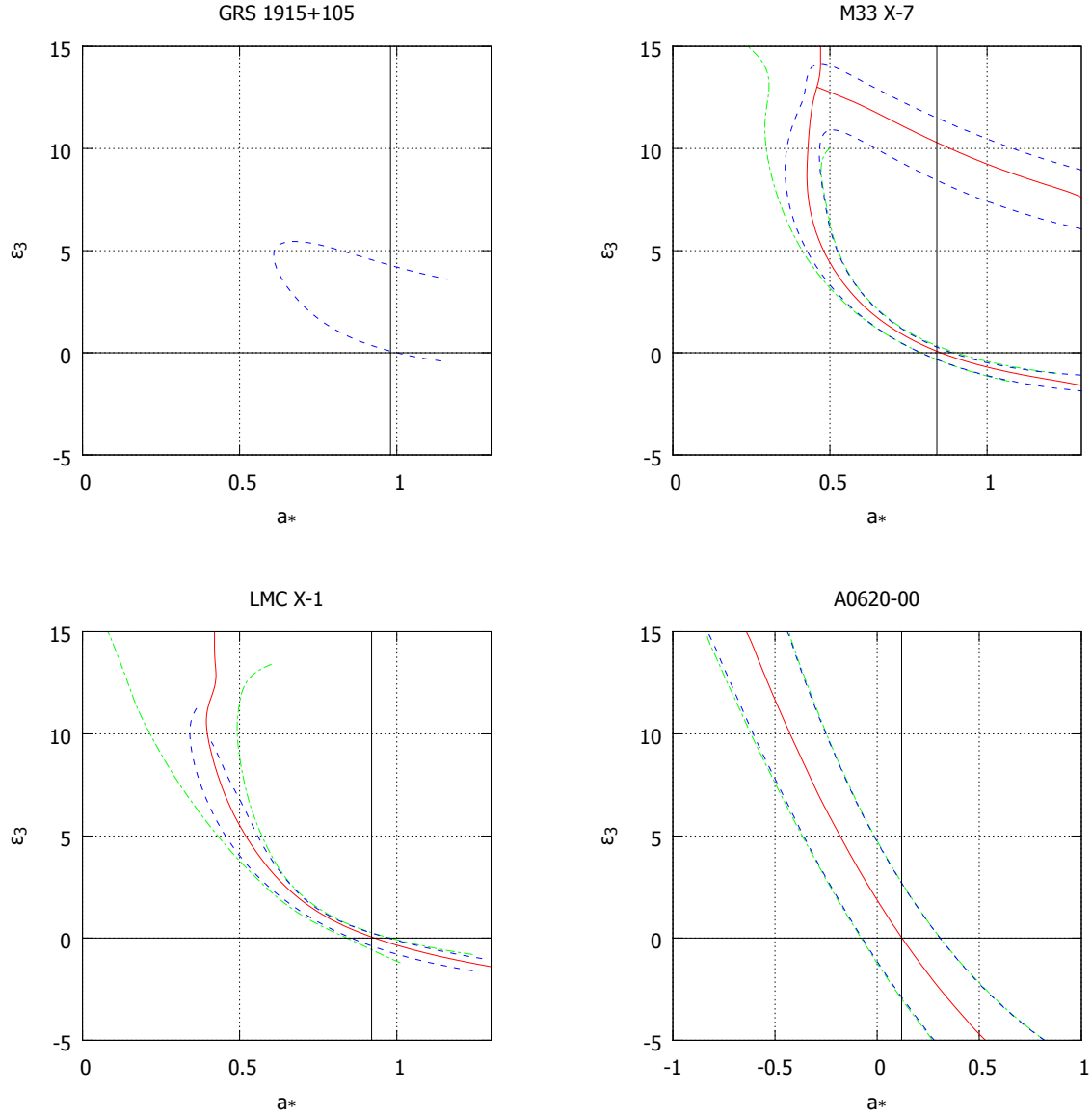


FIG. 2.— As in Fig. 1 for the BH candidates in GRS 1915+105 (top left panel), M33 X-7 (top right panel), LMC X-1 (bottom left panel), and A0620-00 (bottom right panel). See the text for more details.

The different shape of the allowed regions of M33 X-7 and LMC X-1 is due to the different inclination angle (high  $i$  for M33 X-7, low  $i$  for LMC X-1) and the higher value of the spin parameter inferred for LMC X-1. Because of the lower inclination angle, LMC X-1 has not two local minima of  $\chi^2$  in the range under consideration (we would have found the second minimum, as well as the connection point between the two minima, if we had included higher values of  $\epsilon_3$ ). So, the 1-sigma bound  $a_* > 0.87$  inferred in the Kerr background cannot be translated into a bound of  $\epsilon_3$ , in the sense that such a bound is larger than 15, the maximum value of  $\epsilon_3$  shown in our plots. However, because of the higher spin parameter, the blue-dashed lines close before the connection point of the red-solid line. If the BH candidate in LMC X-1 were a Johannsen-Psaltis BH with, for instance,  $\epsilon_3 = 13$ , the analysis of the disk's thermal spectrum under the assumption of Kerr background would provide the spin parameter reported in Tab. 1 for the objects on the red-solid line, but the fit would not be so good. In the case of LMC X-1, the analysis of real data could make the difference, and potentially distinguish a Kerr BH from one with  $\epsilon_3 > 11.5$ .

In the case of the BH candidates in GRS1915+105 and in Cygnus X-1, the Kerr spin measurement is just a lower bound,  $a_* > 0.98$ . For these two objects, the constraints on the spin–deformation parameters plane have been obtained following a slightly different approach. Here the blue-dashed lines separate BHs whose spectrum looks more similar to the one of a Kerr BH with spin parameter higher/lower than 0.98. So, the Kerr bound  $a_* > 0.98$  implies that the region inside these blue-dashed lines is allowed (the spectra of these BHs look like the one of a Kerr BH with spin parameter larger than 0.98), while the one outside is ruled out (the spectra of these BHs would be interpreted as the

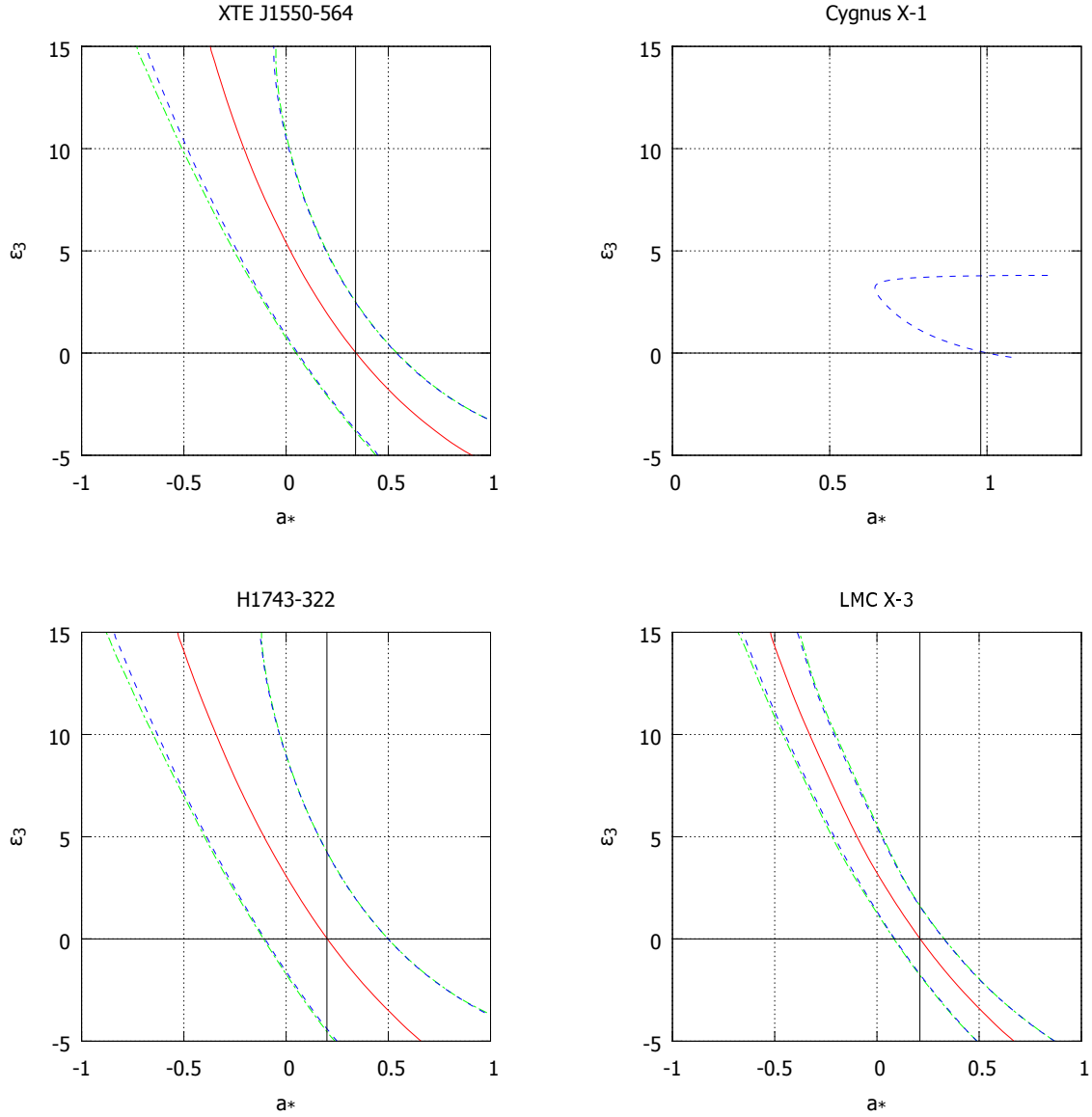


FIG. 3.— As in Fig. 1 for the BH candidates in XTE J1550-564 (top left panel), Cygnus X-1 (top right panel), H1743-322 (bottom left panel), and LMC X-3 (bottom right panel). See the text for more details.

one of a Kerr BH with spin lower than 0.98). The difference between the two plots is just the different inclination angle. The remarkable difference with respect to the other BH candidate constraints is that here the deformation parameter  $\epsilon_3$  turns out to be well constrained. This happens because Johannsen-Psaltis BHs can mimic very fast-rotating Kerr BHs for a quite restricted ranges of the spin and the deformation parameters. In the case of GRS1915+105, the Kerr bound  $a_* > 0.98$  implies  $\epsilon_3 < 6.0$ . For Cygnus X-1, the constraint is  $\epsilon_3 < 4.0$ .

The summary of the spin measurements for some non-vanishing deformation parameter  $\epsilon_3$  are reported in Tab. 2. The spin measurement corresponds to the value of  $\chi_{\min}^2(\epsilon_3)$  (the absolute minimum in the case of M33 X-7). The uncertainties on the spins correspond to the bound provided by the green-dashed-dotted lines. For GRS1915+105 and Cygnus X-1, we report the lower bounds given by their blue-dashed lines.

#### 4. DISCUSSION

In the previous section, we have derived the constraints on the spin parameter  $a_*$  and on the Johannsen-Psaltis deformation parameter  $\epsilon_3$  for the 10 stellar-mass BH candidates for which there is a robust measurement of the spin parameter reported in the literature obtained from the continuum-fitting method and under the assumption of Kerr background. We have not analyzed real X-ray data, but we have used as reference spectrum the one of a Kerr BH



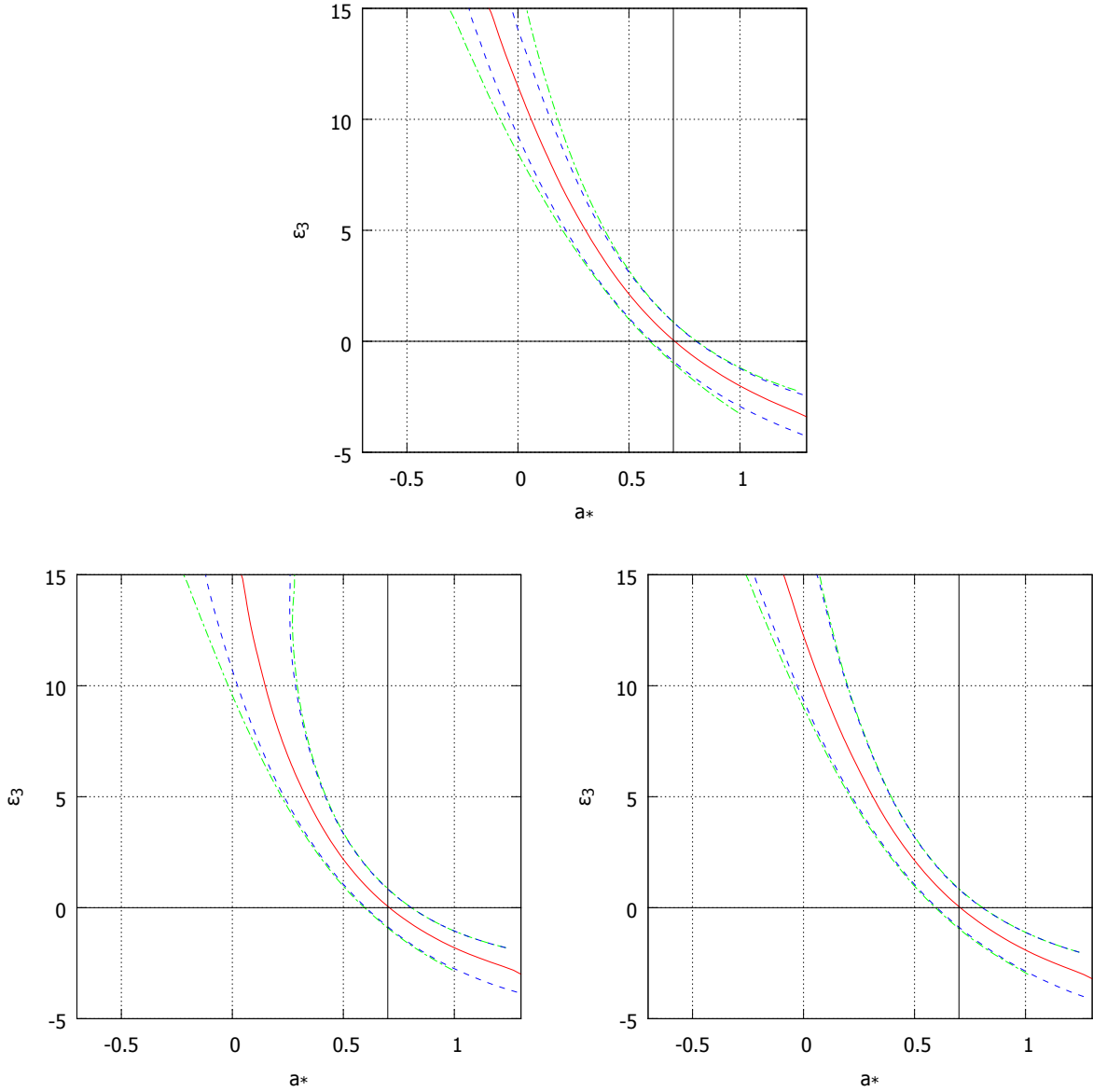


FIG. 4.— Top panel: Disk’s thermal spectrum constraints on possible deviations from the Kerr geometry in the spacetime around the BH candidate in GRO J1655-40 that would have been obtained with an inclination angle  $i = 20^\circ$ . Bottom panels: as in the top panel, using a constant mass accretion rate  $\dot{M} = \dot{M}_0$  instead of  $\dot{M} = \eta_0 \dot{M}_0 / \eta$  in Eq. (13) and an inclination angle  $i = 70.2^\circ$  (left panel) and  $20^\circ$  (right panel). See the text for more details.

with the value of the spin parameter reported in the literature and we have compared this spectrum with the ones expected in the Johannsen-Psaltis background. We would like to stress that our approach can obtain reliable results because, while significantly reducing the time of the analysis as well as all the complications related to a large number of systematic effects, there is no loss of important information. As discussed in more details in Bambi (2012e, 2014), for any Johannsen-Psaltis BH with spin parameter  $a_*$  and deformation parameter  $\epsilon_3$  there is a Kerr BH with different spin parameter but almost indistinguishable disk’s thermal spectrum. In other words, it is usually impossible to distinguish a Kerr from a Johannsen-Psaltis BH from the sole analysis of the thermal spectrum of a thin accretion disk, because there is a sort of degeneracy between the spin and possible deviations from the Kerr solutions. This is usually true for any non-Kerr background and any single observable, not just for the Johannsen-Psaltis metric and the continuum-fitting method (Li & Bambi 2014; Li et al. 2014; Tsukamoto et al. 2014). This result is confirmed by our calculations in the previous section, in which we have found that more often  $\chi_{\min}^2(\epsilon_3) \approx 0$ . From this point of view, the only BH candidate that might benefit of a complete data reanalysis is the object in LMC X-1, for which at high values of  $\epsilon_3$  there is a departure from the spectrum obtained in the Kerr background (the blue-dashed line closes at  $\epsilon_3 \approx 11.5$ ).

The differences between the constraints on the spin-deformation parameters plane found in the previous section for

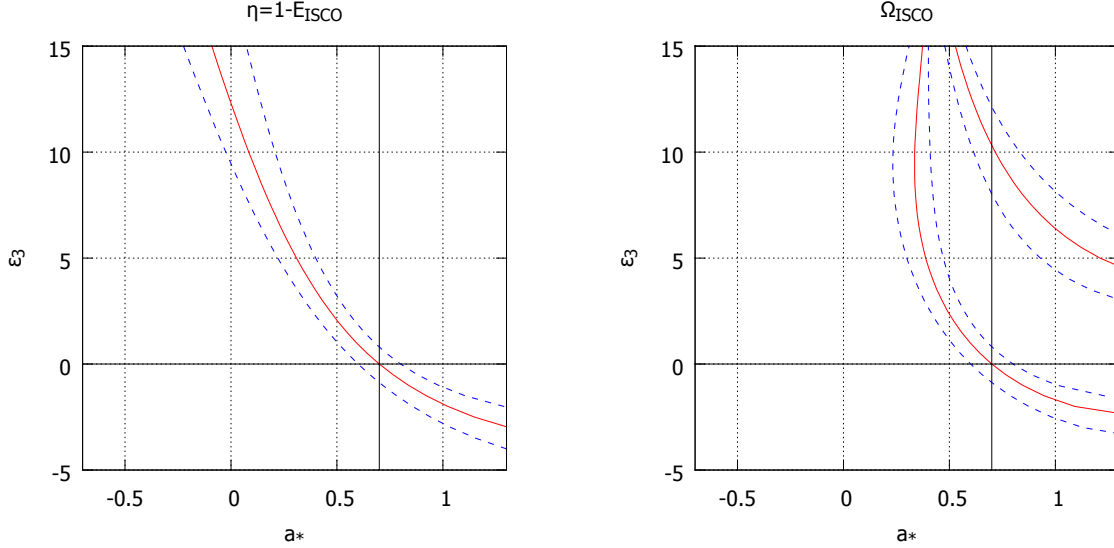


FIG. 5.— Left panel: radiative efficiency in the Novikov-Thorne model  $\eta = 1 - E_{\text{ISCO}}$ . The red-solid line is for  $\eta = 0.1036$ , which is the same as the one for a Kerr BH with  $a_* = 0.7$ . The blue-dashed lines are for  $\eta = 0.0912$  and  $0.1221$ , which correspond, respectively, to the Novikov-Thorne radiative efficiency in Kerr background with  $a_* = 0.6$  and  $0.8$ . Right panel: as in the left panel for the frequency at the ISCO radius. The red-solid lines are for  $\Omega_{\text{ISCO}} = 0.1439$ , while the blue-dashed lines are for  $\Omega_{\text{ISCO}} = 0.1236$  (external lines) and  $0.1737$  (internal lines). In the Kerr background, these values of  $\Omega_{\text{ISCO}}$  correspond, respectively, to  $a_* = 0.7, 0.6$ , and  $0.8$ . See the text for more details.

different BH candidates mainly depend on the measures of the spin parameter inferred in the Kerr background, but a minor role is also played by the value of the disk's inclination angle with respect to our line of sight. The effect of  $i$  becomes more pronounced for  $\epsilon_3 > 10$ : for high values of  $\epsilon_3$ , the preferred spin parameter  $a_*$  is larger for higher  $i$  than the one that would be obtained for lower  $i$ . To make more clear this statement, in the top panel of Fig. 4 we show the continuum-fitting method constraints that would have been obtained for GRO J1655-40 assuming an inclination angle  $i = 20^\circ$  instead of  $i = 70.2^\circ$ . At  $\epsilon_3 = 15$ , the spin measurement for  $i = 20^\circ$  is  $a_* = -0.13_{-0.18}^{+0.10}$ , while for  $i = 70.2^\circ$  one finds  $a_* = 0.17 \pm 0.30$ . For instance, the inclination angle is the key-point for the difference between the shape of the constraints for GRO J1655-40 and 4U 1543-47 in Fig. 1. In the Kerr background, one finds respectively  $a_* = 0.7 \pm 0.1$  and  $a_* = 0.8 \pm 0.1$ ; that is, 4U 1543-47 rotates faster than GRO J1655-40. For high values of the deformation parameter, one finds instead that GRO J1655-40 would rotate faster than 4U 1543-47. The disk's inclination angle is also the only difference between the continuum-fitting method constraints for GRS1915+105 and Cygnus X-1 (top left panel in Fig. 2 and top right panel in Fig. 3).

Concerning the choice of the mass accretion rate, all our constraints have been obtained assuming  $\dot{M}$  given by Eq. (13). In the continuum-fitting method, the mass accretion rate is an output parameter and, even if the correlation with the BH spin is low, some attention has to be taken. The choice in Eq. (13) seems to be the more meaningful because eventually the fit of the thermal spectrum of a thin disk measures the total luminosity  $L = \eta \dot{M}$ . To figure out the effect of a different choice, in Fig. 4 we show the constraints that would have been obtained for GRO J1655-40 in the case of  $\dot{M} = \dot{M}_0$ , respectively for an inclination angle  $i = 70.2^\circ$  (bottom left panel) and  $20^\circ$  (bottom right panel). In the case of a low inclination angle,  $i = 20^\circ$ , one finds more or less the same constraints, see the top panel and the bottom right panel in Fig. 4. For  $i = 70.2^\circ$ , the difference is larger, but only for  $\epsilon_3 > 10$ .

Lastly, let us note that in previous work on tests of the Kerr nature of BH candidates we have used as crude approximation of the continuum-fitting measurements the values of the Novikov-Thorne radiative efficiency  $\eta = 1 - E_{\text{ISCO}}$  (Bambi 2012b,c,d); that is, at first approximation the continuum-fitting method actually measures the radiative efficiency in the Novikov-Thorne model. We thus exploited this fact translating the spin measurements in the Kerr background into radiative efficiency measurements, and then the latter into spin measurements for Johannsen-Psaltis BHs with non-vanishing deformation parameter  $\epsilon_3$ . In the left panel of Fig. 5, we show the constraints that can be obtained with this approximation for the BH candidate in GRO J1655-40. In the Kerr background, the spin measurement is  $a_* = 0.7$  and the 1-sigma lower and upper bounds are, respectively,  $a_* = 0.6$  and  $0.8$ . These three values of the spin parameter correspond to  $\eta = 0.1036, 0.0912$ , and  $0.1221$  in the Kerr metric. In the left panel in Fig. 5, the red-solid line marks the objects with Novikov-Thorne radiative efficiency  $\eta = 0.1036$ , while the blue-dashed lines are for spacetimes with  $\eta = 0.0912$  and  $0.1221$ . The constraints obtained with this simplification (that clearly does not take the inclination angle into account) seem to provide a quite good result if the inclination angle of the disk is low, while there is a more significant departure from the correct measurement in the case of high inclination angles. For instance, for  $\epsilon_3 = 15$  one finds  $a_* = -0.09 \pm 0.15$  from the  $\eta$ -approach, to be compared with the spin measurement  $a_* = -0.13_{-0.18}^{+0.10}$  for the case  $i = 20^\circ$  and the estimate  $a_* = 0.17 \pm 0.30$  for  $i = 70.2^\circ$ . In the right panel

in Fig. 5, we show the contour levels for a Keplerian frequency at the ISCO radius  $\Omega_{\text{ISCO}} = 0.1439$  (red-solid lines) and 0.1236 and 0.1737 (blue-dashed lines). In the case of Kerr background, these values correspond to spacetimes with  $a_* = 0.7, 0.6$  and  $0.8$ , so the case of GRO J1655-40. The radiative efficiency is a better proxy for the continuum-fitting measurements.

## 5. SUMMARY AND CONCLUSIONS

Astrophysical BH candidates are stellar-mass dark objects in X-ray binary system with a mass exceeding the maximum mass for a neutron or quark star and supermassive compact bodies at the center of every normal galaxy. All these objects are thought to be the Kerr BHs predicted in general relativity, but there is not yet an observational confirmation that the spacetime geometry around them is described by the Kerr solution. It is important to stress that the sole observation in their spectra of features associated to relativistic effects absent in Newtonian mechanics is definitively not enough to confirm the Kerr nature of these objects. Non-Kerr BHs may indeed look like Kerr BH with different spin (Bambi 2013d; Li & Bambi 2014; Li et al. 2014; Tsukamoto et al. 2014). The correct way to test the Kerr BH hypothesis is therefore to consider a more general background that includes the Kerr solution as special case. In particular, this more general spacetime will be characterized by a mass  $M$ , a spin parameter  $a_*$ , and at least one deformation parameter. The latter measures possible deviations from the Kerr solution and its numerical value must be inferred from observations. If astrophysical data require a vanishing deformation parameter, the spacetime geometry around the BH candidate is described by the Kerr metric up to a certain level of precision. In the case the outcome is a non-vanishing deformation parameter, the Kerr nature of the BH candidate would be questioned.

In the present paper, we have considered the Johannsen-Psaltis metric with deformation parameter  $\epsilon_3$  as theoretical framework and we have derived the allowed regions on the spin–deformation parameters planes for 10 stellar-mass BH candidates from their continuum-fitting measurements reported in the literature. The continuum-fitting methods is the analysis of the thermal spectrum of geometrically thin and optically thick accretion disks. Assuming that the spacetime around BH candidates is described by the Kerr metric, this technique is used to infer the BH spin parameter  $a_*$ . In the present paper, we have “translated” these spin measurements into allowed regions on the spin–deformation parameters plane. This has been achieved by comparing Kerr spectra with the spin parameters reported in the literature with the spectra computed in Johannsen-Psaltis metric. The approach makes sense because the thermal spectrum of a thin disk around a non-Kerr BH with a certain spin and deformation parameters is extremely similar to the one around a Kerr BH with different spin and that remains true even for quite large deviations from the Kerr solution. In other words, it is impossible even in principle to distinguish a Kerr BH and a non-Kerr BH from the sole analysis of the disk’s thermal spectrum. This approach significantly simplifies our job because we can just focus our attention on the role of the spacetime metric, assuming that all the astrophysical effects and the instrumental issues have been already properly taken into account in the previous studies, and there is not a significant loss of information.

The results of this work are Figs. 1-3 and are summarized in Tab. 2. The constraints obtained here will be combined with other observations in a future work. The most natural choice would be to combine these constraints with measurements of the iron line profile, which is currently the only other relatively robust technique to probe the spacetime geometry around BH candidates and it has been already extended to non-Kerr background in Johannsen & Psaltis (2013); Bambi (2013a). However, only for a few sources we have good X-ray data for both the continuum-fitting method and the analysis of the iron line profile. It is also to be noted that both the techniques strongly rely on the fact that the inner edge of the disk is at the ISCO radius, so their combination may not be the best choice to break the degeneracy between the spin and the deformation parameter and only very good measurement – not available today – could put interesting constraints (Bambi 2013d). A more promising approach could be the combination of the continuum-fitting constraints with current bounds from quasi-periodic oscillations (or QPO) (Johannsen & Psaltis 2011a; Bambi 2012d, 2013e), but at present it is not clear the exact mechanism responsible for these phenomena and different models predict different measurements, which makes this technique not yet mature to test fundamental physics.

This work was supported by the NSFC grant No. 11305038, the Shanghai Municipal Education Commission grant for Innovative Programs No. 14ZZ001, the Thousand Young Talents Program, and Fudan University.

## REFERENCES

- Bambi, C. 2011, *Modern Physics Letters A*, 26, 2453  
 Bambi, C. 2012a, *Phys. Rev. D*, 85, 043001  
 Bambi, C. 2012b, *Phys. Rev. D*, 85, 043002  
 Bambi, C. 2012c, *Phys. Rev. D*, 86, 123013  
 Bambi, C. 2012d, *J. Cosmol. Astropart. Phys.*, 9, 14  
 Bambi, C. 2012e, *ApJ*, 761, 174  
 Bambi, C. 2013a, *Phys. Rev. D*, 87, 023007  
 Bambi, C. 2013b, *The Astronomical Review*, 8, 4  
 Bambi, C. 2013c, *Phys. Rev. D*, 87, 084039  
 Bambi, C. 2013d, *J. Cosmol. Astropart. Phys.*, 8, 55  
 Bambi, C. 2013e, arXiv:1312.2228  
 Bambi, C. 2014, *Physics Letters B*, 730, 59  
 Bambi, C., & Barausse, E. 2011, *ApJ*, 731, 121  
 Bambi, C., & Malafarina, D. 2013, *Phys. Rev. D*, 88, 064022  
 Barausse, E., Cardoso, V., & Khanna, G. 2010, *Physical Review Letters*, 105, 261102  
 Barausse, E., & Sotiriou, T. P. 2008, *Physical Review Letters*, 101, 099001  
 Broderick, A. E., Loeb, A., & Narayan, R. 2009, *ApJ*, 701, 1357  
 Cardoso, V., Pani, P., & Rico, J. 2014, *Phys. Rev. D*, 89, 064007  
 Carter, B. 1971, *Physical Review Letters*, 26, 331

- Chruściel, P. T., Costa, J. L., & Heusler, M. 2012, *Living Reviews in Relativity*, 15, 7
- Dotti, G., Gleiser, R. J., Ranea-Sandoval, I. F., & Vucetich, H. 2008, *Classical and Quantum Gravity*, 25, 245012
- Giacomazzo, B., Rezzolla, L., & Stergioulas, N. 2011, *Phys. Rev. D*, 84, 024022
- Gou, L., McClintock, J. E., Liu, J., et al. 2009, *ApJ*, 701, 1076
- Gou, L., McClintock, J. E., Reid, M. J., et al. 2011, *ApJ*, 742, 85
- Gou, L., McClintock, J. E., Remillard, R. A., et al. 2013, arXiv:1308.4760
- Gou, L., McClintock, J. E., Steiner, J. F., et al. 2010, *ApJ*, 718, L122
- Johannsen, T., & Psaltis, D. 2011a, *ApJ*, 726, 11
- Johannsen, T., & Psaltis, D. 2011b, *Phys. Rev. D*, 83, 124015
- Johannsen, T., & Psaltis, D. 2013, *ApJ*, 773, 57
- Joshi, P. S., Malafarina, D., & Narayan, R. 2014, *Classical and Quantum Gravity*, 31, 015002
- Kalogera, V., & Baym, G. 1996, *ApJ*, 470, L61
- Kolehmainen, M., & Done, C. 2010, *MNRAS*, 406, 2206
- Kormendy, J., & Richstone, D. 1995, *ARA&A*, 33, 581
- Li, L.-X., Zimmerman, E. R., Narayan, R., & McClintock, J. E. 2005, *ApJS*, 157, 335
- Li, Z., & Bambi, C. 2014, *J. Cosmol. Astropart. Phys.*, 1, 41
- Li, Z., Kong, L., & Bambi, C. 2014, arXiv:1401.1282
- Liu, J., McClintock, J. E., Narayan, R., Davis, S. W., & Orosz, J. A. 2008, *ApJ*, 679, L37
- Liu, J., McClintock, J. E., Narayan, R., Davis, S. W., & Orosz, J. A. 2010, *ApJ*, 719, L109
- Maoz, E. 1998, *ApJ*, 494, L181
- McClintock, J. E., Narayan, R., Davis, S. W., et al. 2011, *Classical and Quantum Gravity*, 28, 114009
- McClintock, J. E., Narayan, R., & Rybicki, G. B. 2004, *ApJ*, 615, 402
- McClintock, J. E., Narayan, R., & Steiner, J. F. 2013, *Space Sci. Rev.*, 73
- McClintock, J. E., Shafee, R., Narayan, R., et al. 2006, *ApJ*, 652, 518
- Middleton, M. J., Miller-Jones, J. C. A., & Fender, R. P. 2014, *MNRAS*, 439, 1740
- Morningstar, W. R., Miller, J. M., Reis, R. C., & Ebisawa, K. 2014, *ApJ*, 784, L18
- Narayan, R., & Heyl, J. S. 2002, *ApJ*, 574, L139
- Narayan, R., & McClintock, J. E. 2008, *New Astronomy Reviews*, 51, 733
- Novikov, I. D., & Thorne, K. S. 1973, in *Black Holes*, edited by C. De Witt and B. De Witt (Gordon and Breach, New York, US), 343
- Page, D. N., & Thorne, K. S. 1974, *ApJ*, 191, 49
- Pani, P., Barausse, E., Berti, E., & Cardoso, V. 2010, *Phys. Rev. D*, 82, 044009
- Psaltis, D., Perrodin, D., Dienes, K. R., & Mocioiu, I. 2008, *Physical Review Letters*, 100, 091101
- Remillard, R. A., & McClintock, J. E. 2006, *ARA&A*, 44, 49
- Rhoades, C. E., & Ruffini, R. 1974, *Physical Review Letters*, 32, 324
- Robinson, D. C. 1975, *Physical Review Letters*, 34, 905
- Shafee, R., McClintock, J. E., Narayan, R., et al. 2006, *ApJ*, 636, L113
- Shakura, N. I., & Sunyaev, R. A. 1973, *A&A*, 24, 337
- Steiner, J. F., McClintock, J. E., Orosz, J. A., et al. 2014, arXiv:1402.0148
- Steiner, J. F., McClintock, J. E., & Reid, M. J. 2012, *ApJ*, 745, L7
- Steiner, J. F., Reis, R. C., McClintock, J. E., et al. 2011, *MNRAS*, 416, 941
- Tsukamoto, N., Li, Z., & Bambi, C. 2014, arXiv:1403.0371
- Zhang, S. N., Cui, W., & Chen, W. 1997, *ApJ*, 482, L155